Int. J. Electrochem. Sci., 13 **(2018)** 8376 – 8387, doi: 10.20964/2018.09.53

International Journal of
ELECTROCHEMICAL
SCIENCE
www.electrochemsci.org

Short Communication

Effect of Low Temperature Plasma Nitriding on Salt Spray Corrosion and Electrochemical Corrosion of H13 Hot Work Mould Steel

Zhao Wen, Kong Dejun[*]

School of Mechanical Engineering, Changzhou University, Changzhou 213164, China
[*]E–mail: kong–dejun@163.com

Received: 5 May 2018 / *Accepted:* 26 June 2018 / *Published:* 5 August 2018

A nitrided layer was fabricated on H13 hot work mould steel using a low temperature plasma nitriding (LTPN). The morphologies, distributions of chemical elements and phases of obtained nitrided layer were characterized using a scanning electron microscopy (SEM), energy dispersive spectrometer (EDS) and X–ray diffractometry (XRD), respectively, its nanohardness and modulus of elasticity was measured using a nanoindentation, and its bonding strength was tested using a scratch test. The corrosion properties of substrate and nitrided layer were analyzed using a salt spray corrosion and electrochemical corrosion. The results show that the nitrided layer is primarily composed of nitrides, whose nanohardness and modulus of elasticity is 11.0 and 213.0 GPa, respectively, and the average bonding strength of nitrided layer is 50.23 N measured by scratch test, showing high bonding strength between the nitrided layer and the substrate. The corrosion products on the substrate and nitrided layer after SSC are γ–FeOOH and α–FeOOH, of which the α–FeOOH prevents further the nitride layer and substrate from corrosion. The corrosion potential of substrate and nitrided layer is –0.79 and –0.65 V, respectively, exhibiting that the nitrided layer has higher electrochemical corrosion resistance. The capacitive impedance loop of nitrided layer is significantly larger than that of substrate, its lowest measurement frequency $|Z|_{0.01Hz}$ and low–frequency phase angle values are also greater than the substrate, showing that the nitrided layer is acted as an effective anti–corrosion barrier layer to prevent corrosive ions from entering into the substrate, which increases its electrochemical corrosion resistance.

Keywords: low temperature plasma nitriding (LTPN); nitrided layer; salt spray corrosion (SSC); electrochemical corrosion; corrosion mechanism

1. INTRODUCTION

As a hot work mould steel, H13 steel is widely used in the manifesting of hot forging, hot extrusion and die casting due to its high hardenability, strength and toughness [1–2]. However, in the

absence of working, H13 steel is prone to occurring environmental corrosions such as salt spray corrosion and electrochemical corrosion in humid state, which greatly shortens its service life and increases the production costs [3]. Therefore, it is particularly important to improve its corrosion resistance property under the extreme humid conditions [4, 5]. A lot of researches on surface technologies have been carried out in China and abroad. Lu et al [6] analyzed the effect of electron beam (EB) polishing technology on the surface quality of $3Cr_2Mo$ plastic mould steel; Nazir et al [7] simulated the corrosion–wear performance of nickel–graphene composite coating; Bai et al [8] investigated the chlorine–induced corrosion of high–velocity oxygen fuel (HVOF) sprayed β–NiAl coating. The above researches tried to improve the corrosion resistance of substrate by various methods such as electron beam polishing, composite coating and HVOF, but there are few reports on the corrosion resistance of nitrided layer using a low temperature plasma nitriding (LTPN), which is a process that enhances the hardness and corrosion performance of H13 steel by forming the nitrides of Cr, V and Mo. Due to its characteristics of environmental friendliness and economical application, the LTPN becomes a popular surface modification technology in the past decades [9, 10].

In this study, a nitrided layer was fabricated on H13 hot work mould steel using a low temperature plasma nitriding (LTPN). The morphologies and phases of obtained nitrided layer were analyzed using a scanning electron microscopy (SEM) and X–ray diffractometry (XRD), respectively, and the bonding strength, nanohardness and modulus of elasticity were measured using a scratch and nanoindentation test, respectively. The effects of LTPN on salt spray corrosion and electrochemical corrosion of nitrided layer were analyzed to investigate the corrosion resistance mechanism of nitrided layer.

2. EXPERIMENTAL

2.1 Sample preparation

The substrate was H13 hot work mould steel with the chemical compositions: C 0.32–0.45%, Si 0.80–1.20%, Mn 0.20–0.50%, Cr 4.75–5.50%, Mo 1.10–1.75%, V 0.80–1.20%, P ≤0.030%, S ≤0.030%, the rest was Fe. The quenching and tempering process was quenching at 1080 °C in oil and tempering at 560 °C for 2 h. After heat treatment, the samples were mechanically polished and ultrasonic cleaning in the acetone for 15 min. The LTPN test was performed on a IVA type vacuum nitriding furnace, technological parameters: temperature of 450 °C, time of 10 h, volume ratio of nitrogen to hydrogen of 2: 1, nitrogen flow of 40 $mL•min^{-1}$, pressure of 400–500 Pa.

2.2 Characterization method

After the nitriding test, the surface and cross–section morphologies of obtained nitrided layer were analyzed using a JSM–6360LA type scanning electron microscope (SEM), its phases were analyzed using a D/max 2500 PC type X–ray diffractometer (XRD). The nanohardness and modulus of elasticity of nitrided layer were measured using a G200 type nanoindentation tester, technological

parameters: pressure head of Berkovich, continuous stiffness mode, and maximum displacement of 2000 nm. The bonding strength of nitrided layer was characterized using a WS–2005 type film scratch tester, test parameters: load of 0–60 N, loading speed of 100 N/min, scratch speed of 4 mm/min.

The salt spray corrosion test was performed on an YQW–250 type salt spray corrosion (SSC) chamber. The test conditions: spray medium of 3.5 wt.% NaCl solution, test period of 720 h. After the SSC test, the morphologies and chemical corrosion products were analyzed using a JSM–6360LA type SEM and its configured EDS, respectively.

The electrochemical test was carried out on a CHI660E type electrochemical workstation, the commonly three–electrode system, platinum electrode were used as auxiliary electrode, saturated calomel electrode (SCE) as a reference electrode, the sample (nitrided and original) as a working electrode, the scan rate of potentiodynamic test was 0.001 V/s. The electrochemical impedance spectroscopy was performed at an open circuit potential, the electrochemical impedance spectroscopy data was analyzed and processed using a ZSimpWin software.

3. ANALYSIS AND DISCUSSION

3.1 Characterization of surface and cross–sections

3.1.1 Surface and cross–section morphologies

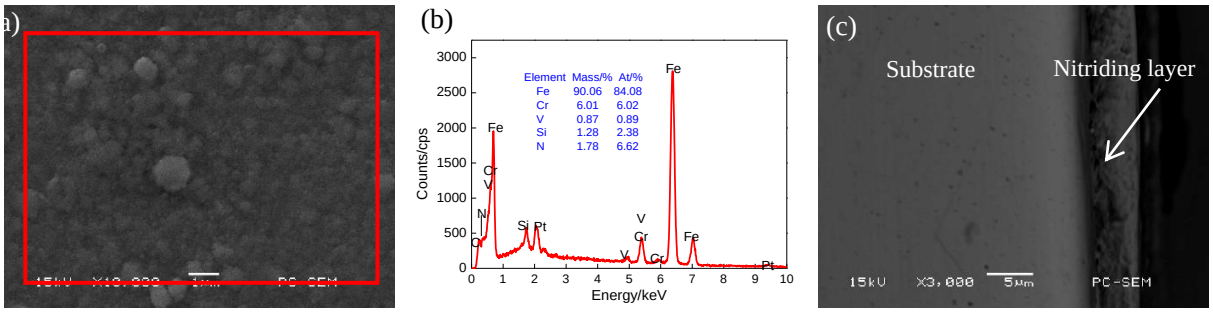

Figure 1. Morphologies and EDS analysis of nitrided layer (a) Surface morphology, (b) Result of EDS analysis, (c) Cross–section morphology

The morphology of nitrided layer surface is shown in Fig.1 (a). The nitrided layer was covered by some spherical nitride particles, with no obvious defects such as porosity and cracks. The spherical protrusions were caused by the deposition of nitride particles due to sputtering of cathode surface [11]. The EDS analysis result of nitrided layer is shown in Fig.1 (b), and the scanned position was the part enclosed by the red box. The nitrided layer was primarily composed of Fe, Cr, V, Si, and N, in which the Fe, Cr, V and Si originated from the substrate, while the N came from the nitrogen–contained compounds (including nitrogenous martensite, γ'–Fe_4N and ε–$Fe_{2–3}N$) produced in the nitriding process [2]. After the LTPN test, the average micro–hardness of nitrided layer (1144.33 HV) was 2.49 times than that of substrate (459.53 HV), improving its wear resistance. As shown in Fig.1 (c), the nitrided layer was composed of compound layer and diffused zone, there was an obvious demarcation between

the nitrided layer and the substrate. The compound layer (composed of γ'–Fe_4N and ε–$Fe_{2-3}N$) was a clear white bright layer, whose thickness was related to the concentration of nitrogen in the nitriding gas, temperature and time. The diffusion zone was the left zone of bright white layer, which consisted of nitrogenous martensite through the austenite–martensite phase.

3.1.2 XRD analysis

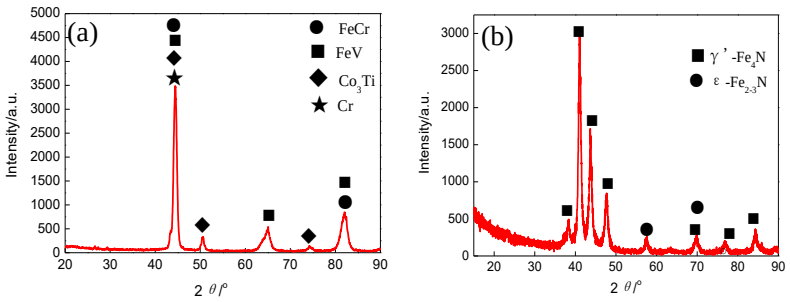

Figure 2. XRD phase analysis of substrate and nitrided layer (a) Substrate, (b) Nitrided layer

Fig.2 shows the XRD spectra of substrate and nitrided layer. The substrate was primarily composed of FeCr, FeV, Co_3Ti and Cr, as shown in Fig.2 (a), while the nitrided layer consisted of nitride phases, primarily γ'–Fe_4N and ε–$Fe_{2-3}N$ phases. The nitrides of Cr, Si and V were not observed due to their small content [12], as shown in Fig.2 (b).

3.1.3 Nanomechanical properties

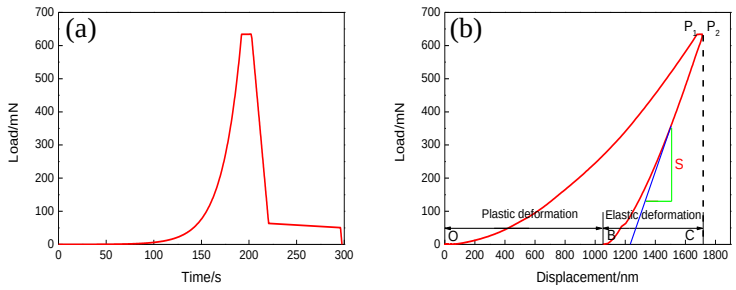

Figure 3. Nanoindentation curves of nitrided layer (a) Loads vs time, (b) Loads vs displacements

Fig.3 (a) shows the curve of load vs time. The load increased from 0 to the maximum value in a non–linear manner, the loading speed also gradually increased in the loading process. When the load reached the maximum value, the test entered the maintenance period (constant load), lasted for 20 s, the nitrided layer produced a slight creep effect at this period [13]. At the end of maintenance period, the indenter was unloaded at a constant unloading speed. However, the unloading speed suddenly became very slow at 10% of peak load, which was to ensure that the contact between the nitrided layer and the indenter was maintained.

Fig.3 (b) shows the curve of load vs displacement. The curves of OP_1 and P_2B were the loading

and unloading periods, respectively. At the loading period, the elastic and plastic deformations occurred simultaneously, the applied load increased with the penetration depth, while only the elastic deformation occurred at the unloading period. During the loading and unloading periods, the curves were continuous, there was no "pop in" and "elbow" phenomenon, indicating that the nitrided layer did not crack during the nanoindentation test [14, 15]. As shown in Fig.3 (b), there were two closed regions, namely the region OP_1P_2B (A_1 represented its area) and the region OP_1P_2C (A_2 represented its area), which represented the plastic deformation work (W_p) and the total deformation work (W_t), respectively. According to literatures [16] and [17], the ratio ($\eta_p=A_1/A_2=W_p/W_t$) was defined as a plasticity factor. The smaller the value of η_p, the greater the resistance of plastic deformation was. The calculated plasticity factor η_p of nitrided layer was 58.231%, which was less than 60%, indicating that the nitrided layer had better corrosion resistance but less plasticity. As shown in Fig.3 (b), the stiffness value of S was defined as the slope on the unloading curve. The Oliver and Pharr method [18] calculated the nanohardness and modulus of elasticity of nitrided layer was 11.06 and 213.00 GPa, respectively. The H/E and H^3/E^2 was 0.052 and 0.030, respectively, indicating that the nitrided layer had high wear resistance and plastic deformation resistance, which was consistent with the conclusion drawn from the η_p [16].

3.2 Salt spray corrosion

3.2.1 Plane scan analysis of corrosion products

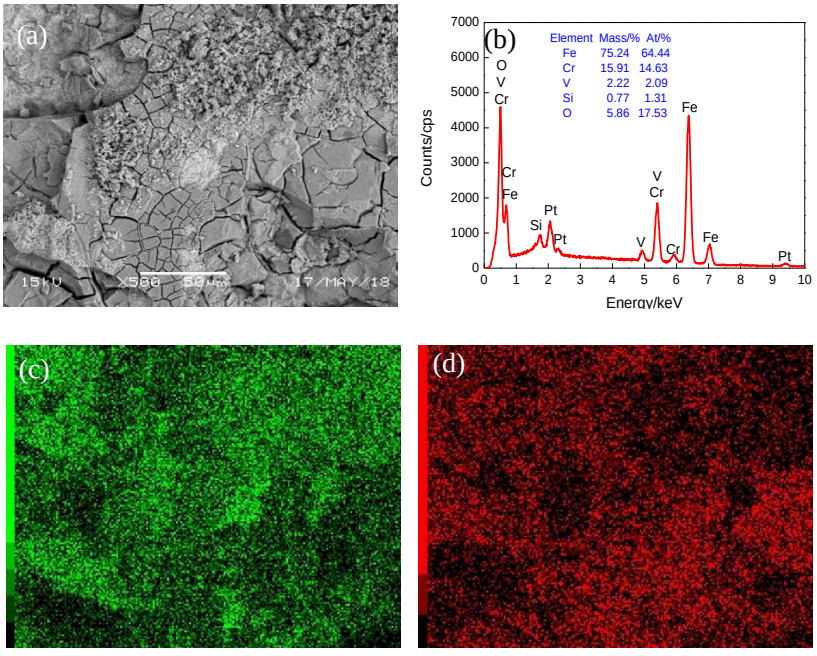

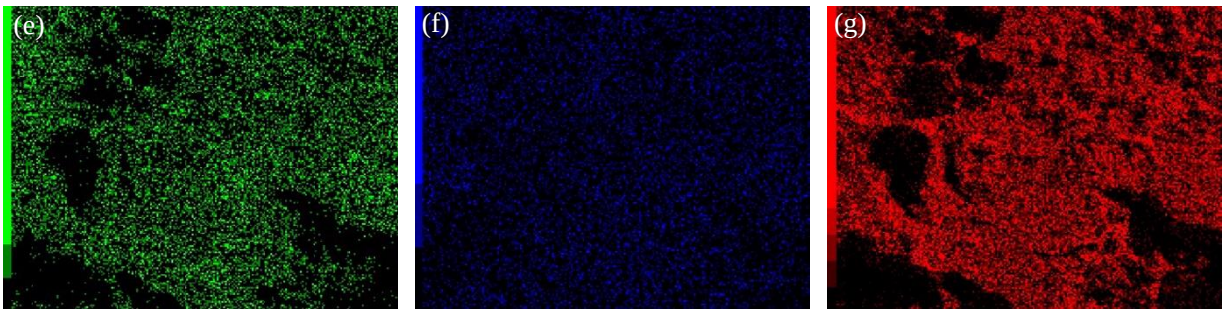

Figure 4. Plane scan analysis of substrate after SSC with 3.5 wt.% NaCl solution (a) Plane scanned position, (b) Result of plane san analysis, (c) Fe content, (d) Cr content, (e) Si content, (f) V content, (g) O content

Fig.4 (a) shows the plane scanned position of substrate after SSC. During the SSC test, the Fe ions combined with the chloride ions to produce the corrosion products, which were dissolved in water. Some corrosion products flowed away with the salt spray, so that the corrosion continued. With the reaction continuing, the oxide layer became thicker and blocked the diffusion of chloride ions, at the same time, the substrate surface was cracked due to the stress caused by the accumulation of corrosion products. The result of plane scan analysis is shown in Fig.4 (b). The Fe, Cr and Si was discontinuously distributed, which formed the atoms–rich zones on the substrate surface and the atoms–poor zones on the corrosion pits and peeled parts, as shown in Fig.4 (c)–(e), indicating that the substrate experienced the severe corrosion. The V was uniformly distributed on the corrosion product surface due to its low content, as shown in Fig.4 (f). The O distribution was the same as that of Fe, Cr and Si, which was derived from their oxides, as shown in Fig.4 (g), indicating that more corrosion products were formed and the corrosion was severe.

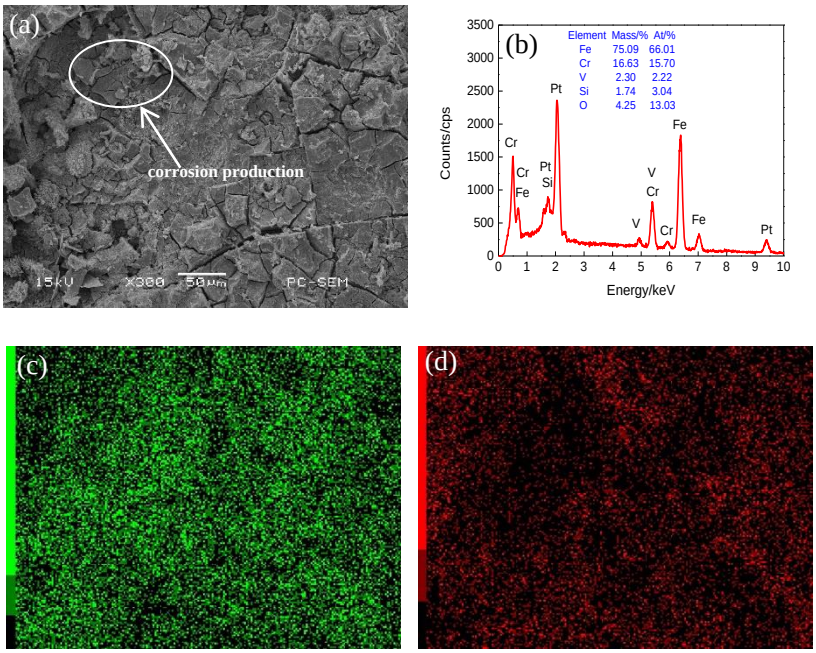

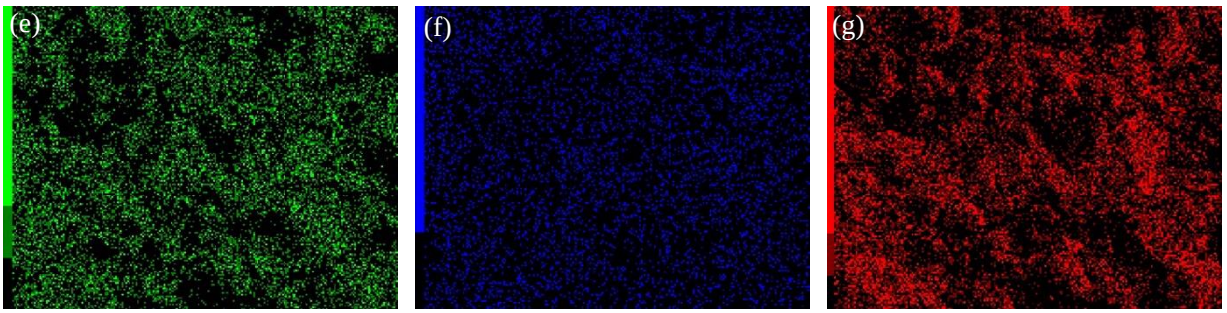

Figure 5. Plane scan analysis of nitrided layer after SSC with 3.5 wt.% NaCl solution (a) Plane scanned position, (b) Result of plane scan analysis, (c) Fe content, (d) Cr content, (e) Si content, (f) V content, (g) O content

Fig.5 (a) shows the plane scanned position of nitrided layer after SSC. The crevice corrosion and peeling corrosion occurred on the nitrided layer surface, which was covered with corrosion products. The corrosion cracks also existed on the nitrided layer, which was related to the brittleness of ε–$Fe_{2-3}N$ phase formed by LTPN [19]. The result of plane scan analysis is shown in Fig.5 (b). The Cl and Na was not found due to their low contents. The Fe, Cr and Si were also discontinuously distributed on the nitrided layer, which formed the atoms–rich zones on the nitrided layer and the atoms–poor zones on the corrosion pits, as shown in Fig.5 (c)–(e), indicating that the pits and peelings were produced on the oxide film surface, which affected the distributions of Fe, Cr and Si. The V were uniformly distributed, there was no atoms–rich zones, as shown in Fig.5 (f), indicating that the V corrosion products were dissolved in corrosion solution during the corrosion reaction. The O formed the atoms–rich zones on the oxides of Fe, Cr and Si, which had a certain protection effect on preventing further corrosion, as shown in Fig.5 (g).

3.2.2 Corrosion morphologies and XRD analysis

The dissolution of Fe occurred on the anode in NaCl solution, while the oxygen reduction process occurred on the cathode. The intermediate product of $Fe(OH)_2$ formed in the initial period of corrosion was oxidized and dehydrated after further contacting with the air to form the FeOOH, which was further dehydrated to form the Fe_2O_3 [20].

On the anode, the Fe lost electron to form the Fe^{2+} [21], i.e.

$$Fe \rightarrow Fe^{2+} + 2e^- \quad (1)$$

On the cathode, the O_2 gained electron to produce the OH^- with the H_2O, i.e.

$$1/2O_2 + H_2O + 2e^- \rightarrow 2OH^- \quad (2)$$

The Fe^{2+} in Eq.(1) was reacted with the OH^- in Eq.(2) to produce the $Fe(OH)_2$ as follows:

$$Fe^{2+} + 2OH^- \rightarrow Fe(OH)_2 \quad (3)$$

The $Fe(OH)_2$ in Eq.(3) was further oxidized into the $Fe(OH)_3$, i.e.

$$2Fe(OH)_2 + 1/2O_2 + H_2O \rightarrow 2Fe(OH)_3 \quad (4)$$

The whole transformation process was shown as follows:

$$Fe(\text{II})\ (Fe(OH)_2, Fe_3O_4) \xrightarrow{\text{Rapid oxidation}} Fe(\text{III})\ (FeOOH) \xrightarrow{\text{Dehydration}} Fe_2O_3 \quad (5)$$

The γ–FeOOH formed a relatively complete protective layer and had a certain blocking effect

on chloride ions, as shown in Fig.6 (a). However, the whiskers on the surface of α–FeOOH did not formed and the content of α–FeOOH was relatively less, as shown in Fig.6 (b). Since the α–FeOOH had a certain protective ability to the substrate [22], the above incomplete conversion of α–FeOOH had a negative effect on the improvement of SSC performance of substrate. Fig.6 (c) shows the XRD analysis of substrate after SSC. Obviously, the corrosion products at this time existed mainly in the form of iron oxides, which were the Fe_3O_4 and $FeCr_2O_4$ phases.

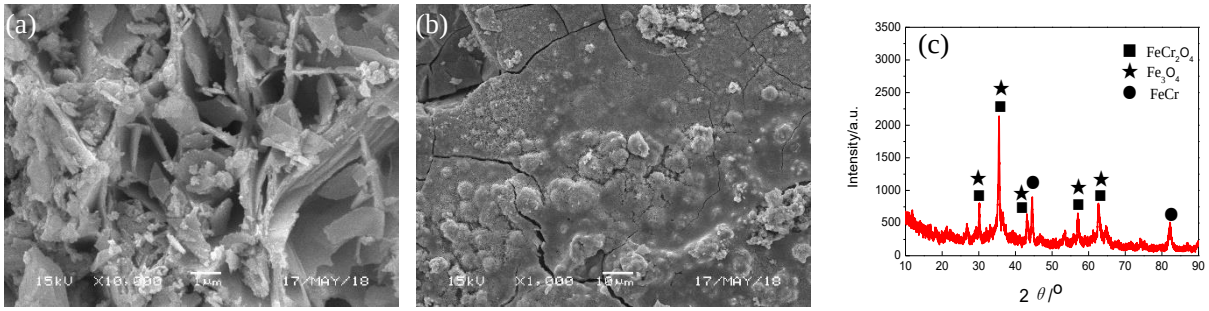

Figure 6. Morphologies and XRD analysis of corrosion products on substrate after SSC with 3.5 wt.% NaCl solution (a) Lamellar morphology, (b) Cotton spheroidal morphology, (c) XRD analysis

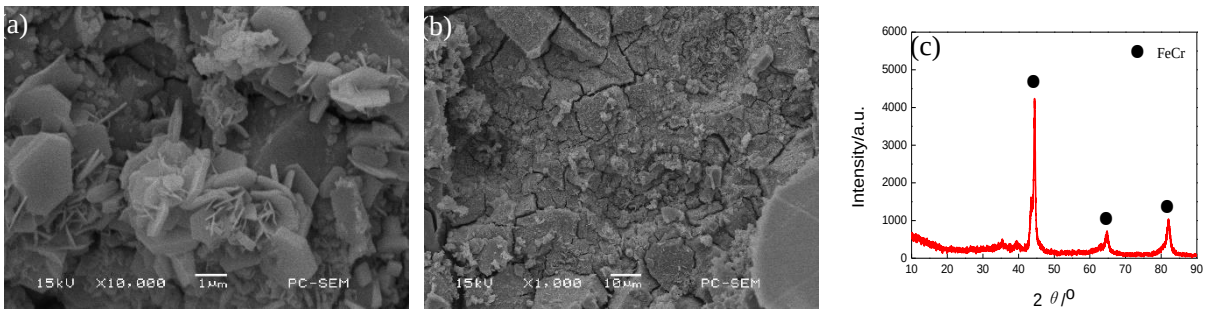

Figure 7. Morphologies and XRD analysis of corrosion products on nitrided layer after SSC with 3.5 wt.% NaCl solution (a) Lamellar morphology, (b) Cotton spheroidal morphology, (c) XRD analysis

The corrosion products on the nitrided layer were the same as those on the substrate, which were γ–FeOOH (Fig.7 (a)) and α–FeOOH (Fig.7 (b)). However, compared to the γ–FeOOH generated on the substrate, the size of γ–FeOOH also generated on the nitrided layer was reduced due to the partial conversion of γ–FeOOH to α–FeOOH. In the case of low Cl^- concentration, the Cl^- favored the conversion of γ–FeOOH to α–FeOOH [22, 23], no β–FeOOH was found on the corrosion products [23]. The α–FeOOH produced by the corrosion of nitrided layer was more complete, the intact α–FeOOH had a lower electrochemical activity, high adhesion and compactness, and a certain protective effect on the nitrided layer [24, 25]. Fig.7 (c) shows the XRD analysis of nitrided layer after SSC. The oxide phases were not detected, which was due to the few corrosion products. Compared with XRD analysis, it can be found that the nitrided layer had higher SSC resistance than the substrate.

3.3 Electrochemical corrosion

3.3.1 Polarization curves

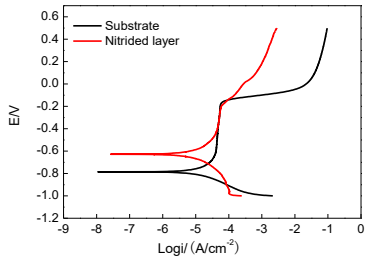

Figure 8. Polarization curves of substrate and nitrided layer in 3.5 wt.% NaCl solution

The polarization curves of substrate and nitrided layer in 3.5 wt.% NaCl solution are shown in Fig.8. When the scanned potential exceeded the corrosion potential (E_{corr}), the current density rapidly increased with the potentials increasing. As the potential exceeded –0.70 V, the growth rate of current density began to slow down and maintained a high current density, the passivation region appeared on the polarization curve. While the potential exceeded –0.20 V, the current density increased significantly with the potentials increasing, indicating that the substrate surface was again exposed to the corrosion solution after the passivation film was penetrated.

The polarization parameters of substrate and nitrided layer are shown in Table 1. The E_{corr} and corrosion current density (I_{corr}) of substrate was –0.79 V and 1.61×10^{-5} A•cm^{-2}, respectively, while the E_{corr} and I_{corr} of nitrided layer was –0.65 V and 7.33×10^{-6} A•cm^{-2}, respectively. The I_{corr} of nitrided layer was lower than that of substrate, indicating that the nitrided layer had a lower corrosion rate than the substrate, at the same time, the E_{corr} of nitrided layer was higher than that of substrate, indicating that the nitrided layer had a higher corrosion resistance than the substrate.

Table 1. Polarization parameters of substrate and nitrided layer in 3.5 wt.% NaCl solution

Parameter	E_{corr}/V	I_{corr}/A•cm^{-2}
Substrate	–0.79	1.61×10^{-5}
Nitrided layer	–0.65	7.33×10^{-6}

3.3.2 Impedance spectrum

Fig.9 shows the equivalent circuit models of substrate and nitrided layer. The equivalent circuit of substrate showed a time constant, the physical model ($R(QR)$) with coating capacitor in parallel was used to fit the equivalent circuit (R_e, R_s and Q_s represented electrolyte resistance, substrate resistance and substrate capacitance, respectively). In the phase angle graph of nitrided layer (Fig.10 (b)), the maximum values of two phase angles were presented. Accordingly, their data were fitted to the $R(Q(R(QR)))$ equivalent circuit with two time constants, indicating that the corrosion solution had reached the interface of nitrided layer/substrate through the micro–defects in the nitrided layer and

formed a corrosion micro–cell at the interface zones. In the fitting circuit, R_{pl} and Q_{pl} represented the resistance and capacitance of porous layer, respectively, R_t represented the charge transfer resistance at the interface of nitrided layer porosity/substrate, and Q_{dl} represented the electric double layer capacitance in the nitrided layer porosity/substrate interface.

Table 2 lists the fitting results of electrochemical impedance spectroscopy (EIS) measurements of substrate and nitrided layer. The R_s (R_t) values on the substrate and nitride layer were 8953 and 14670 Ω•cm^2, respectively, obviously, the nitride layer had a higher value. The higher R_s values (R_t value on the equivalent circuit of nitride layer) meant higher electrochemical corrosion resistance [26], it was concluded that the nitrided layer was more corrosion resistant than the substrate because

Table 2. Equivalent circuit parameters of substrate and nitrided layer in 3.5 wt.% NaCl solution

Parameter	R_e/Ω•cm^2	Q_{pl}/F•cm^{-2}	R_{pl}/Ω•cm^2	$Q_s(Q_{dl})$/F•cm^{-2}	R_s (R_t)/Ω•cm^2
Substrate	60.84	–	–	7.702×10^{-5}	8953
Nitrided layer	85.84	4.872×10^{-5}	3909	3.246×10^{-4}	14670

Fig.10 (a) shows the Nyquist diagram of substrate and nitrided layer. The *Z*' represented the real part of impedance corresponded to the resistance part of impedance, while the *Z*'' represented the imaginary part of impedance corresponded to the capacitive part of impedance. It was well known that the size of capacitive impedance loop was proportional to the resistance of corrosion reaction, i.e., the corrosion resistance was better when the radius of capacitive impedance loop was larger [27, 28, 29]. Therefore, the Nyquist diagram showed that the nitrided layer had higher corrosion resistance.

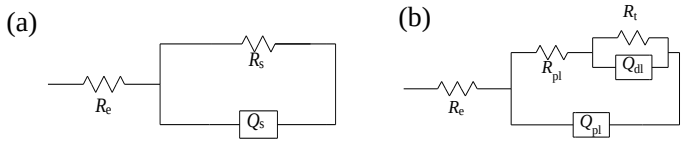

Figure 9. Equivalent circuit models of substrate and nitrided layer in 3.5 wt.% NaCl solution (a) Substrate, (b) Nitrided layer

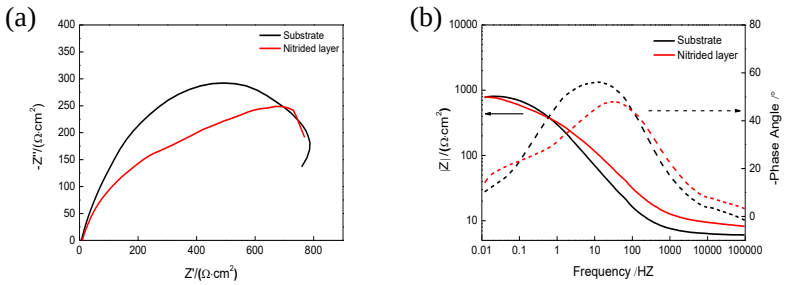

Figure 10. EIS analysis of substrate and nitrided layer in 3.5 wt.% NaCl solution (a) Nyquist diagram, (b) Bode diagram

On the Bode–impedance diagram in Fig.10 (b), the high frequency region was related to local surface defects and solution resistance, while the intermediate frequency region represented the occurring processes on the passivation film, and the low frequency region represented the occurring process at the coating/substrate interface [30]. The impedance modulus at the lowest measurement frequency ($|Z|_{0.01Hz}$) was often used as a semi–quantitative indicator of barrier layer [31]. According to Bode diagram, the nitrided layer showed a slightly higher $|Z|_{0.01Hz}$ than the substrate, which meant that the nitrided layer was used as an effective anti–corrosion barrier layer. The low–frequency phase angle of nitrided layer was higher than that of substrate, indicating that the intrusion resistance of corrosive ions was greater at the nitrided/electrolyte interface.

4 CONCLUSIONS

(1) The low–temperature plasma nitrided layer is composed of spherical nitride grains, its nanohardness and elastic modulus is 11.06 and 213.00 GPa, respectively, which increases its corrosion resistance and plastic deformation resistance.

(2) The cracks and spalling on the nitrided layer are less than that on the substrate, the corrosion product of complete α–FeOOH is formed after SSC, which is used as a protective layer to prevent the further corrosion, the nitrided layer has better SSC resistance than the substrate.

(3) The corrosion potential (E_{corr}) and corrosion current density (I_{corr}) of substrate is –0.79 V and 1.61×10^{-5} A•cm^{-2}, respectively, and that of nitrided layer is –0.65 V and 7.33×10^{-6} A•cm^{-2}, respectively, that the nitrided layer has slower corrosion rate and higher corrosion resistance than the substrate.

(4) The Nyquist plot and Bode plot shows that the nitrided layer is acted as an effective corrosion barrier layer to improve the electrochemical corrosion resistance of substrate.

ACKNOWLEDGEMENTS
Financial support for this research by the Key Research and Development Project of Jiangsu Province (BE2016052) is gratefully acknowledged.

References

1. D. Papageorgiou, C. Medrea and N. Kyriakou, *Eng. Fail. Anal.*, 35 (2013) 355
2. S.D. Jacobsen, R. Hinrichs, C. Aguzzoli, C.A. Figueroa, I.J.R. Baumvol and M.A.Z. Vasconcellos, *Surf. Coat. Technol.*, 286 (2016) 129
3. G. Telasang, J.D. Majumdar, G. Padmanabham and I. Manna, *Surf. Coat. Technol.*, 261 (2015) 69
4. A.A.C. Recco and A.P. Tschiptschin, *J. Mater. Res. Technol.*, 1 (2012) 182
5. N.S. Bailey, C. Katinas and Y.C. Shin, *J. Mater. Process. Technol.*, 247 (2017) 223
6. J. Lu, D. Wei, R. Wang, X. Sui and J. Yin, *Vacuum*, 143 (2017) 283
7. M.H. Nazir, Z.A. Khan, A. Saeed, A. Siddaiah and P.L. Menezes, *Tribol. Int.*, 121 (2018) 30
8. M. Bai, L. Reddy and T. Hussain, *Corros. Sci.*, 135 (2018) 147
9. S.L. Li, C.Y. Ma, Q.Y. Zhang, C.S. Ren and W.Q. Lu, *Surf. Coat. Technol.*, 309 (2016) 47

10. B. Miao, Y. Chai, K. Wei and J. Hu, *Vacuum*, 133 (2016) 54
11. H. Aghajani, M. Torshizi and M. Soltanieh, *Vacuum*, 141 (2017) 97
12. Y. Li, Z. Wang and L. Wang, *Appl. Surf. Sci.*, 298 (2014) 243
13. D. Panfil, M. Kulka, P. Wach, J. Michalski and D. Przestacki, *J. Alloy Compds.*, 706 (2017) 63
14. K. Liu, M. Ostadhassan and B. Bubach, *J. Nat. Gas Sci. Eng.*, 35 (2016) 1310
15. S. Xu, P. Munroe, J. Xu and Z.H. Xie, *Surf. Coat. Technol.*, 307 (2016) 470
16. F. Zhang, M. Yan, J. He and F. Yin, *Vacuum*, 142 (2017) 106
17. Y.Q. Wu and M.F. Yan, *Vacuum*, 86 (2011) 119
18. W.C. Oliver and G.M. Pharr, *J. Mater. Res.*, 7 (1992) 1564
19. C. Nouveau, P. Steyer, K.R.M. Rao and D. Lagadrillere, *Surf. Coat. Technol.*, 205 (2011) 4514
20. B. Panda, R. Balasubramaniam and G. Dwivedi, *Corros. Sci.*, 50 (2008) 1684
21. Z. Wang, J. Liu, L. Wu, R. Han and Y. Sun, *Corros. Sci.*, 67 (2013) 1
22. Y. Ma, Y. Li and F. Wang, *Corros. Sci.*, 51 (2009) 997
23. T. Ishikawa, R. Katoh, A. Yasukawa, K. Kandori, T. Nakayama and F. Yuse, *Corros. Sci.*, 43 (2001) 1727
24. X.Q. Cheng, Y.W. Tian, X.G. Li and C. Zhou, *Mater. Corros.*, 65 (2014) 1033
25. Y. Zhao, H. Ren, H. Dai and W. Jin, *Corros. Sci.*, 53 (2011) 1646
26. J. Alphonsa, V.S. Raja and S. Mukherjee, *Corros. Sci.*, 100 (2015) 121
27. S.P. Mani and N. Rajendran, *Energy*, 133 (2017) 1050
28. M. Gao, W. Lu, B. Yang, S. Zhang and J. Wang, *J. Alloy Compds.*, 735 (2018) 1363
29. J.Z. Lu, B. Han, C.Y. Cui, C.J. Li and K.Y. Luo, *Opt. Laser Technol.*, 88 (2017) 250
30. N.D. Nam, D.S. Jo, J.G. Kim and D.H. Yoon, *Thin Solid Films*, 519 (2011) 6787
31. Z.H. Wen, Y. Bai, J.F. Yang and J. Huang, *J. Alloy Compds.*, 711 (2017) 659